Backstepping Fault Tolerant Control for Double Star Induction Machine under Broken Rotor Bars

Noureddine Layadi[1*], Samir Zeghlache[2], Ali Djerioui[1], Hemza Mekki[3], Fouad Berrabah[1], Azeddine Houari[4] and Mohamed-Fouad Benkhoris[4]

1- Department of Electrical Engineering, Laboratoire de génie Electrique, University Mohamed Boudiaf of M'Sila, BP 166, Ichbilia 28000, Algeria.
Email: layadinoureddine1@gmail.com (Corresponding author)
Email: alidjerioui@yahoo.fr
Email: Fouadberrabah1@gmail.com

2- Department of Electronics, Laboratoire d'Analyse des Signaux et Systèmes, University Mohamed Boudiaf of M'Sila, BP 166, Ichbilia 28000, Algeria.
Email: zegsam5@gmail.com

3- Ecole National Polytechnique, Automatic Control Department LCP, B.P 182 Elharrach, Algiers, Algeria.
Email: hamza.mekki@g.enp.edu.dz

4- IREENA Laboratory, University of Nantes, Saint-Nazaire, France.
Email: Azeddine.Houari@univ-nantes.fr
Email: Mohamed-Fouad.Benkhoris@univ-nantes.fr

Received: August 2018 Revised: January 2019 Accepted: April 2019

ABSTRACT:
In this paper a Passive Fault Tolerant Control (PFTC) based on non-linear backstepping control is proposed for a Double Star Induction Machine (DSIM) under Broken Rotor Bars (BRB) fault of a squirrel-cage in order to improve its reliability and availability. The proposed PFTC is able to maintain acceptable performance in the event of BRB. This control technique guarantees robustness against uncertainties and external disturbances and is also able to deal directly with faults by compensating for the effects of the BRB fault in the machine without prior knowledge on the fault, its location and its severity. The stability of the closed-loop is verified by the exploitation of the Lyapunov theory. a comparative study is made between the proposed Fault Tolerance Control (FTC) and Sliding Mode Control (SMC) for demonstrating the performance and effectiveness of the proposed controller. The results obtained show that the proposed FTC has a better robustness against the BRB fault where the DSIM operates with acceptable performance in both speed and torque.

KEYWORDS: Double Star Induction Machine, Backstepping Control, Sliding Mode Control, Fault Tolerant Control, Broken Rotor Bars.

1. INTRODUCTION

The Double Star Induction Machine (DSIM) belongs to the category of Multiphase Induction Machines (MIM). It has been selected as the best choice because of its many advantages over its three-phase counterpart. The DSIM has been proposed for different fields of industry that need high power such as electric hybrid vehicles, locomotive traction, ship propulsion and many other applications where the safety condition is required such as aerospace and offshore wind energy systems. DISM not only guarantees a decrease of rotor harmonics currents and torque pulsations but it also has many other advantages such as: reliability, power segmentation and higher efficiency. DSIM has a greater fault tolerance; it can continue to operate and maintain rotating flux even with open-phase faults thanks to the greater number of degrees of freedom that it owns compared to the three-phase machines [1-2].

The traditional squirrel cage is subject to various faults that diminish its performance, such as broken rotor bars, end ring connectors and eccentricities. For this reason, there is a major benefit to develop fault tolerant control that compensates for the effect of broken bars, the passive form is preferred in this case because it is both robust and simple to implement. Squirrel cage Induction Motors (IMs) are the most used in the industry with a percentage of 85% [3]. Due to their permanent use, IMs are subject to various faults such as bearing faults (40%–50%), rotor faults (5%–10%) stator faults (30%–40%) [4]. A Broken Rotor Bar (BRB) increases the intensity of currents flowing in

adjacent bars, which provokes the augmentation of the mechanical efforts and subsequently the breaking of the corresponding bars and can also cause defects in the stator [5]. The main factors causing the BRB fault are: mechanical cracks or thermal stress, rotor fabrication process and overloads [6].

The appearance of the BRB fault decreases the performance of the machine but does not cause the immediate stop, for this reason, various diagnoses are used to detect the broken bar fault in the squirrel cage rotor of the induction motor. These detection methods are based on the analysis of the signals of the machine as: motor currents, electromagnetic torque, flux, instantaneous power and mechanical vibration. Despite its drawbacks to the voltage source in case of voltage harmonic distortion, the Motor Current Signature Analysis (MCSA) method is largely used to detect a broken rotor bar [7]. Usually, The MCSA is used to detect electrical and mechanical faults in induction machines because of its simplicity and efficiency; MCSA does not require additional sensors; it is based solely on the analysis of reliable information provided by stator currents at start-up or in steady state.

The Fault Tolerance Control (FTC) allows a machine to continue to operate with satisfactory performance even in the event of defects. In the literature, there are two fault-tolerant control methods: Passive Fault-Tolerant Control (PFTC) and Active Fault-Tolerant Control (AFTC). PFTC uses robust control techniques to preserve the stability of the system with an acceptable level of performance when the fault appears, the system continues to operate with the same control structure, usually, this method is used when the fault diagnosis is difficult to acquire. On the other hand, AFTC is based on online fault compensation and needs real-time information about faults, consequently, this approach requires reconfiguration based on the information provided by the Fault Detection and Identification (FDI) block [8-10].

The occurrence of a BRB fault in a double star induction machine can cause serious damage to the machine itself and related equipment and, as a result, cause a sudden shutdown of industrial processes resulting in significant economic losses, for this reason, a fault tolerant control is mandatory for the DSIM because it allows the system to continue to function properly after the occurrence of the fault and thus provides great economic benefits to the industry. In this paper, the backstepping control technique is chosen for its closed-loop robustness against parametric variation and for its high fault tolerance when applied to an induction motor with defective rotor [11]. It is also chosen for its best transient and steady state performance when applied on a five-phase induction machine [12-13]. The design of BSC controllers that impose parameter tracking and drive the closed-loop system with stable behavior is performed in three stages using the appropriate gains that satisfy the asymptotic stability. The overall stability of the DSIM controlled by the proposed FTC is then verified using Lyapunov's theory. The proposed FTC is tested in healthy and defective conditions with other control methods recently applied on a six-phase induction machine [14-15]. The performance of the two control strategies is studied and compared in terms of robustness against BRB fault. In addition, this paper made several contributions in terms of fault modeling, control strategy, type of machine processed and type of fault:

- A new faulty model design of DSIM is presented in this paper, it is about a modeling of the BRB fault in the d-q reference frame, this fault simulation is precise and closer to the real defect, and moreover, it facilitates the development of any control strategy.
- In this study, the development of an FTC for a DSIM with a BRB fault is carried out for the first time.
- Compared to [16-18], the proposed FTC does not need fault detection and isolation schemes, which avoids estimation errors.
- Compared to work in [11], the application of the proposed FTC on a DSIM is more advantageous because nowadays the multiphase induction machine is more used than the traditional induction motor as a centerpiece in several important areas of the industry.
- Compared with [19-20], the degree of severity of the fault dealt with in this paper is more important since open phase fault tolerance is a specific feature of multiphase machines thanks to the high number of phases that belong to it.

After the introduction, this paper is organized as follows: the following section describes the healthy model of DSIM and establishes the state equations in d-q reference frame. Section 3 models the defective model of the DSIM. Backstepping control design for DSIM is carried out in section 4. Simulation results and their discussions are given in section 5. The last section is reserved for conclusion.

2. DSIM HEALTHY MODEL

The DSIM is composed of two stators shifted by an electric angle and a mobile squirrel cage rotor. Each stator is composed of three uniformly distributed immovable windings whose axes are offset from each other by an electric angle equal to $2\pi/3$. Fig. 1 shows an explicit schematic of the stator and rotor windings, α is the angle shift between the two stators, it is usually equal to 30° and θ is the angle between rotor and stator1 [2]. In order to establish the mathematical

model of DSIM, the following assumptions are made: air-gap uniform, magnetic linearity, negligible saturation and stators are identical.

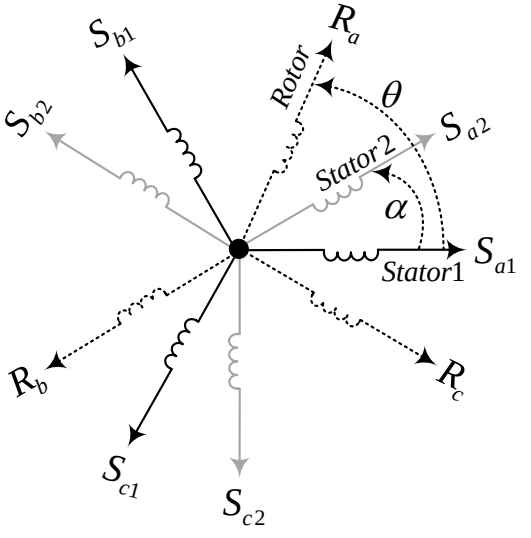

Fig. 1. The DSIM windings.

The d-q dynamic healthy model of squirrel cage double star induction machine with a reference frame fixed to the rotor is given by:

$$\frac{d}{dt}i_{sd1} = \frac{1}{L_{s1}}\left\{v_{sd1} - R_{s1}i_{sd1} + \omega_s\left(L_{s1}i_{sq1} + T_r\varphi_r\omega_{gl}\right)\right\} \quad (1)$$

$$\frac{d}{dt}i_{sq1} = \frac{1}{L_{s1}}\left\{v_{sq1} - R_{s1}i_{sq1} - \omega_s\left(L_{s1}i_{sd1} + \varphi_r\right)\right\} \quad (2)$$

$$\frac{d}{dt}i_{sd2} = \frac{1}{L_{s2}}\left\{v_{sd2} - R_{s2}i_{sd2} + \omega_s\left(L_{s2}i_{sq2} + T_r\varphi_r\omega_{gl}\right)\right\} \quad (3)$$

$$\frac{d}{dt}i_{sq2} = \frac{1}{L_{s2}}\left\{v_{sq2} - R_{s2}i_{sq2} - \omega_s\left(L_{s2}i_{sd2} + \varphi_r\right)\right\} \quad (4)$$

$$\frac{d}{dt}\omega_r = \frac{1}{J}\left[p^2\frac{L_m}{L_m + L_r}\varphi_r\left(i_{sq1} + i_{sq2}\right) - pT_L - K_f\omega_r\right] \quad (5)$$

$$\frac{d}{dt}\varphi_r = \frac{-1}{t_r}\varphi_r + \frac{L_m}{t_r}\left(i_{sd1} + i_{sd2}\right) \qquad / t_r = \frac{L_m + L_r}{R_r} \quad (6)$$

The electromagnetic torque equation is given by:

$$T_e = p\frac{L_m}{L_m + L_r}\left[\varphi_{rd}\left(i_{sq1} + i_{sq2}\right) - \varphi_{rq}\left(i_{sd1} + i_{sd2}\right)\right] \quad (7)$$

Where v_{sd1}, v_{sq1} are stator1 voltages components. v_{sd2}, v_{sq2} are stator2 voltages components. i_{sd1}, i_{sq1} are stator1 currents components. i_{sd2}, i_{sq2} are stator2 currents components. L_{s1}, L_{s2}, L_r and L_m are stator1, stator2, rotor and mutual inductance, respectively. R_{s1}, R_{s2} and R_r are respectively stator1, stator2 and rotor resistance. $T_r = L_r/R_r$ is the rotor time constant. T_L is the applied load torque. ω_r is the rotor speed. J, K_f denote the rotor inertia and friction coefficient. ω_s is the stator pulsation. ω_{gl} is the slip pulsation. φ_r is the rotor flux. p denotes the number of pole pairs. The subscripts d, q designate direct and quadrate indices according to the usual d-q axis components in the synchronous rotating frame.

3. DSIM FAULTY MODEL

To simulate a BRB(s) fault in the double star induction machine, we increase the resistance of a rotor phase by a value "e" [21], therefore, the defective squirrel cage rotor is represented by an unbalanced three-phase system as shown in Fig .2.

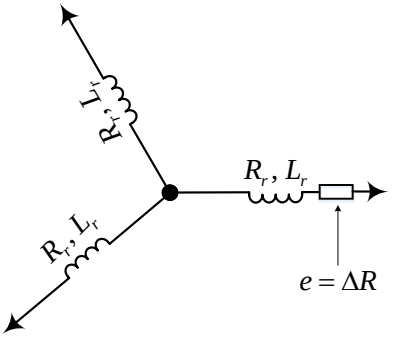

Fig. 2. Simulation of BRB in DSIM.

Substituting R_r with $R_r + e$ in (1), (3) and (6), we find the defective model of the DSIM:

$$\frac{d}{dt}i_{sd1} = \frac{1}{L_{s1}}\left\{v_{sd1} - R_{s1}i_{sd1} + \omega_s\left(L_{s1}i_{sq1} + \frac{L_r}{R_r}\varphi_r\omega_{gl}\right)\right\} + h_1(x) \quad (8)$$

$$\frac{d}{dt}i_{sq1} = \frac{1}{L_{s1}}\left\{v_{sq1} - R_{s1}i_{sq1} - \omega_s\left(L_{s1}i_{sd1} + \varphi_r\right)\right\} \quad (9)$$

$$\frac{d}{dt}i_{sd2} = \frac{1}{L_{s2}}\left\{v_{sd2} - R_{s2}i_{sd2} + \omega_s\left(L_{s2}i_{sq2} + T_r\varphi_r\omega_{gl}\right)\right\} + h_2(x) \quad (10)$$

$$\frac{d}{dt}i_{sq2} = \frac{1}{L_{s2}}\left\{v_{sq2} - R_{s2}i_{sq2} - \omega_s\left(L_{s2}i_{sd2} + \varphi_r\right)\right\} \quad (11)$$

$$\frac{d}{dt}\omega_r = \frac{1}{J}\left[p^2\frac{L_m}{L_m + L_r}\varphi_r\left(i_{sq1} + i_{sq2}\right) - pT_L - K_f\omega_r\right] \quad (12)$$

$$\frac{d}{dt}\varphi_r = -\frac{R_r}{L_m + L_r}\varphi_r + \frac{R_r L_m}{L_m + L_r}\left(i_{sd1} + i_{sd2}\right) + h_3(x) \quad (13)$$

Where $h_1(x)$, $h_2(x)$ and $h_3(x)$ represent the fault terms due to the BRB fault (rotor resistance variation), they are given by:

$$\begin{cases} h_1(x) = -\dfrac{\omega_s \varphi_r \omega_{gl} L_r e}{R_r (R_r + e) L_{s1}} \\ h_2(x) = -h_1(x) \dfrac{L_{s1}}{L_{s2}} \\ h_3(x) = -\dfrac{e}{L_m + L_r} \varphi_r + \dfrac{e L_m}{L_m + L_r} (i_{sd1} + i_{sd2}) \end{cases} \quad (14)$$

4. BACKSTEPPING CONTROL DESIGN

The objective of the proposed passive FTC is to lead the rotor electrical speed ω_r and the rotor flux φ_r to their desired references under both load torque disturbance T_L and broken rotor bars without the need for reconfiguration or an FDI block, this can only be achieved if the load torque disturbance T_L and the terms produced by the BRB fault are bounded and their bounds are known, in this study the proposed FTC consists of three steps, in each step, an adaptive function of Lyapunov is associated in order to ensure the stability of the closed-loop system, the final function of Lyapunov related to the stability of the overall system is the sum of all Lyapunov functions. For the compensation of uncertainties in each subsystem, the sign function is used. Since the stabilizing function is required to be continuously differentiable, the sign function is approximated by the hyperbolic function tanh [11]. In this section, the actual load torque is assumed to be bounded by a fixed maximum value $T_L^{\max}$ and the functions $h_i(x)$ are also bounded by $H_i^{\max}$, $i = \overline{1,3}$.

4.1. Step1: Flux Control

The aim of this step is to lead the flux φ_r to a desired reference φ_r^*. The tracking error of flux is:

$$e_\varphi = \varphi_r - \varphi_r^* \quad (15)$$

Deriving (15), we obtain:

$$\dot{e}_\varphi = \dot{\varphi}_r - \dot{\varphi}_r^* \quad (16)$$

Using (6), (16) becomes:

$$\dot{e}_\varphi = \left(\frac{-R_r}{L_r + L_m} \varphi_r + \frac{L_m R_r}{L_r + L_m} (i_{sd1} + i_{sd2}) + h_3(x) - \dot{\varphi}_r^* \right) \quad (17)$$

The Lyapunov function candidate is defined as:

$$V_\varphi = e_\varphi^2 / 2 \quad (18)$$

The derivative of (18) according to the time is:

$$\dot{V}_\varphi^{g} = e_\varphi \dot{e}_\varphi = e_\varphi \left(\frac{-R_r}{L_r + L_m} \varphi_r + \frac{L_m R_r}{L_r + L_m} (i_{sd1} + i_{sd2}) + h_3(x) - \dot{\varphi}_r^* \right) \quad (19)$$

The desired value of $(i_{sd1} + i_{sd2})$ named i_{sd}^* which stabilizes the flux and makes $\dot{V}_\varphi$ negative defined is chosen as follows:

$$i_{sd}^* = \frac{L_r + L_m}{L_m R_r} \left(-k_\varphi e_\varphi - k_1 \tanh\left(\frac{k_1 h}{\xi_1} e_\varphi\right) + \frac{R_r}{L_r + L_m} \varphi_r + \dot{\varphi}_r^* \right) \quad (20)$$

Where $k_1 > 0$, $k_\varphi > 0$, $\xi_1 > 0$ and $h = 0.2785$ (according to lemma 1 of [11]).

We admit that:

$$i_{sd1}^* = i_{sd2}^* = i_{sd}^* / 2 \quad (21)$$

Proof of stability of i_{sd}^*:

Replacing $(i_{sd1} + i_{sd2})$ by i_{sd}^* in (17), we obtain:

$$\dot{V}_\varphi = -k_\varphi e_\varphi^2 - k_1 \tanh\left(\frac{k_1 h}{\xi_1} e_\varphi\right) e_\varphi + h_3(x) e_\varphi \quad (22)$$

For $k_1 > H_3^{\max}$, we can make the following inequality:

$$\dot{V}_\varphi^{g} \le -k_\varphi e_\varphi^2 - k_1 \tanh\left(\frac{k_1 h}{\xi_1} e_\varphi\right) e_\varphi + k_1 |e_\varphi| \quad (23)$$

With

$$|e_\varphi| = e_\varphi \, sign(e_\varphi) \quad (24)$$

Replacing (24) into (23), the derivative of the Lyapunov function becomes:

$$\dot{V}_\varphi \le -k_\varphi e_\varphi^2 - k_1 \tanh\left(\frac{k_1 h}{\xi_1} e_\varphi\right) e_\varphi + k_1 e_\varphi \, sign(e_\varphi) \quad (25)$$

Equation (25) can be written as follows [11]:

$$\dot{V}_\varphi \le -k_\varphi e_\varphi^2 + \xi_1 \quad (26)$$

On the other hand, we have:

$$\left|\frac{\partial V_\varphi}{\partial e_\varphi}\right| = |e_\varphi| \le |e_\varphi| + b_\varphi \qquad \forall b_\varphi > 0 \tag{27}$$

According to theorem 1 of [11], (26) and (27) imply that the error e_φ is globally uniformly exponentially practically stable; it converges to a ball whose radius can be reduced by making small the setting parameter ξ_1.

4.2. Step2: Speed Control

The aim of this step is to steer the speed ω_r to a desired reference ω_r^* . The tracking error of speed is:

$$e_\omega = \omega_r - \omega_r^* \tag{28}$$

The error dynamic of the speed is:

$$\dot{e}_\omega = \dot{\omega}_r - \dot{\omega}_r^* \tag{29}$$

Using (5), (29) becomes:

$$\dot{e}_\omega = \frac{p^2}{J}\frac{L_m}{L_m + L_r}\varphi_r\left(i_{sq1} + i_{sq2}\right) - \frac{p}{J}T_L - \frac{K_f}{J}\omega_r - \dot{\omega}_r^* \tag{30}$$

The Lyapunov function candidate adapted to the speed is defined as:

$$V_\omega = \frac{1}{2}e_\omega^2 \tag{31}$$

The derivative of (31) according to the time is:

$$\dot{V}_\omega = e_\omega \dot{e}_\omega = e_\omega\left(\frac{p^2}{J}\frac{L_m}{L_m + L_r}\varphi_r\left(i_{sq1} + i_{sq2}\right) - \frac{p}{J}T_L - \frac{K_f}{J}\omega_r - \dot{\omega}_r^*\right) \tag{32}$$

In order to make the controller robust against the load torque disturbance, the desired value of $(i_{sq1} + i_{sq2})$ named i_{sq}^* which adjusts the speed and makes $\dot{V}_\omega$ negative defined is chosen as follows:

$$i_{sq}^* = \frac{J\left(L_m + L_r\right)}{p^2 L_m \varphi_r}\left(-k_\omega e_\omega - k_2 \tanh\left(\frac{k_2 h}{\xi_2}e_\omega\right) + \frac{K_f}{J}\omega_r + \dot{\omega}_r^*\right) \quad \varphi_r \neq 0 \tag{33}$$

With $k_2 > 0$, $k_\omega > 0$, $\xi_2 > 0$ and $h = 0.2785$. We also admit that:

$$i_{sq1}^* = i_{sq2}^* = i_{sq}^* / 2 \tag{34}$$

Proof of stability of i_{sq}^* :

Replacing $(i_{sq1} + i_{sq2})$ by i_{sq}^* in (32), we obtain:

$$\dot{V}_\omega = e_\omega \dot{e}_\omega = e_\omega\left[-k_\omega e_\omega - k_2 \tanh\left(\frac{k_2 h}{\xi_2}e_\omega\right) - \frac{p}{J}T_L\right] \tag{35}$$

$$\dot{V}_\omega = -k_\omega e_\omega^2 - k_2 \tanh\left(\frac{k_2 h}{\xi_2}e_\omega\right)e_\omega - e_\omega\frac{p}{J}T_L \tag{36}$$

For $k_2 \ge \frac{p}{J}T_L^{\max}$, we can make the following inequality:

$$\dot{V}_\omega \le -k_\omega e_\omega^2 - k_2 \tanh\left(\frac{k_2 h}{\xi_2}e_\omega\right)e_\omega + k_2|e_\omega| \tag{37}$$

With

$$|e_\omega| = e_\omega sign(e_\omega) \tag{38}$$

Replacing (38) into (37), the derivative of the Lyapunov function becomes:

$$\dot{V}_\omega \le -k_\omega e_\omega^2 + \xi_2 \tag{39}$$

On the other hand, we have:

$$\left|\frac{\partial V_\omega}{\partial e_\omega}\right| = |e_\omega| \le |e_\omega| + b_\omega \qquad \forall b_\omega > 0 \tag{40}$$

Equations (39) and (40) confirm that the error e_ω is globally uniformly exponentially practically stable; it converges to a ball whose radius can be reduced by making small the setting parameter ξ_2 .

4.3. Step3: Current Control

In this step, the control law is established by forcing the four stator currents: i_{sd1}, i_{sq1}, i_{sd2} and i_{sq2} generated by the two previous steps to reach their desired references i_{sd1}^*, i_{sq1}^*, i_{sd2}^* and i_{sq2}^* respectively. Stator current errors are defined as follows: $e_{isd1} = i_{sd1} - i_{sd1}^*$, $e_{isq1} = i_{sq1} - i_{sq1}^*$, $e_{isd2} = i_{sd2} - i_{sd2}^*$ and $e_{isq2} = i_{isq2} - i_{isq2}^*$ .The dynamics of the tracking errors of the currents are:

$$\dot{e}_{isd1} = \frac{v_{sd1}}{L_{s1}} - \frac{R_{s1}}{L_{s1}}i_{sd1} + \omega_s i_{sq1} + \frac{T_r\varphi_r\omega_s\omega_{gl}}{L_{s1}} - \frac{\tau_r}{2L_m}\ddot{\varphi}_r^* -$$

$$\frac{\tau_r}{2L_m}F_1(e_\varphi)\left(\frac{L_m}{\tau_r}i_{sd}-\frac{1}{\tau_r}\varphi_r\right)+\frac{\tau_r}{2L_m}\left[F_1(e_\varphi)-\frac{1}{\tau_r}\right]\dot{\omega}_r^*+$$
$$h_1(x)-\frac{\tau_r}{2L_m}F_1(e_\varphi)h_3(x) \quad (41)$$

$$\dot{i}_{sq1}=\frac{v_{sq1}}{L_{s1}}-\frac{R_{s1}}{L_{s1}}i_{sq1}-\omega_s i_{sd1}-\frac{\omega_s\varphi_r}{L_{s1}}-F_2(e_\omega,\omega,\varphi_r)-$$
$$\frac{J(L_m+L_r)}{2p^2L_m\varphi_r}F_1(e_\omega)\left(\frac{p^2L_m}{J(L_m+L_r)}i_{sq}\varphi_r-\frac{K_f}{J}\omega_r\right)-$$
$$\frac{(L_m+L_r)K_f^2}{2p^2JL_m\varphi_r}\ddot{\omega}_r^*+\frac{(L_m+L_r)F_1(e_\omega)}{2pL_m\varphi_r}T_L+$$
$$\frac{J(L_m+L_r)}{2p^2L_m\varphi_r}\dot{\omega}_r^*\left(F_1(e_\omega)-\frac{K_f}{J}\right) \quad (42)$$

$$\dot{i}_{sd2}=\frac{v_{sd2}}{L_{s2}}-\frac{R_{s2}}{L_{s2}}i_{sd2}+\omega_s i_{sq2}+\frac{T_r\varphi_r\omega_s\omega_{gl}}{L_{s2}}-\frac{\tau_r}{2L_m}\ddot{\varphi}_r^*-$$
$$\frac{\tau_r}{2L_m}F_1(e_\varphi)\left(\frac{L_m}{\tau_r}i_{sd}-\frac{1}{\tau_r}\varphi_r\right)+\frac{\tau_r}{2L_m}\left[F_1(e_\varphi)-\frac{1}{\tau_r}\right]\dot{\omega}_r^*+$$
$$h_2(x)-\frac{\tau_r}{2L_m}F_1(e_\varphi)h_3(x) \quad (43)$$

$$\dot{i}_{sq2}=\frac{v_{sq2}}{L_{s2}}-\frac{R_{s2}}{L_{s2}}i_{sq2}-\omega_s i_{sd2}-\frac{\omega_s\varphi_r}{L_{s2}}-F_2(e_\omega,\omega,\varphi_r)-$$
$$\frac{J(L_m+L_r)}{2p^2L_m\varphi_r}F_1(e_\omega)\left(\frac{p^2L_m}{J(L_m+L_r)}i_{sq}\varphi_r-\frac{K_f}{J}\omega_r\right)+$$
$$\frac{J(L_m+L_r)}{2p^2L_m\varphi_r}\dot{\omega}_r^*\left(F_1(e_\omega)-\frac{K_f}{J}\right)-\frac{(L_m+L_r)K_f^2}{2p^2JL_m\varphi_r}\ddot{\omega}_r^*+$$
$$\frac{(L_m+L_r)F_1(e_\omega)}{2pL_m\varphi_r}T_L \quad (44)$$

The dynamic errors $\dot{e}_\varphi$ and $\dot{e}_\omega$ can be rewritten according to e_d and e_q:

$$\begin{cases}\dot{e}_\varphi=-k_\varphi e_\varphi+\dfrac{L_m}{\tau_r}e_d-k_1\tanh(\dfrac{k_1h}{\xi_1}e_\varphi)+h_3(x)\\ \dot{e}_\omega=\dfrac{p^2}{J}\dfrac{L_m}{L_m+L_r}\varphi_r e_q-\dfrac{p}{J}T_L-k_\omega e_\omega-\\ k_2\tanh(\dfrac{k_2h}{\xi_2}e_\omega)\end{cases} \quad (45)$$

With:

$$\begin{cases}e_d=i_{sd}-i_{sd}^*\\ e_q=i_{sq}-i_{sq}^*\end{cases} \quad (46)$$

Where:

$$F_1(e_\omega)=-k_\omega-\frac{k_2^2h}{\xi_2}(1-\tanh(\frac{k_2h}{\xi_2}e_\omega)^2)+\frac{K_f}{J} \quad (47)$$

$$F_1(e_\varphi)=-k_\varphi-\frac{k_1^2h}{\xi_1}(1-\tanh(\frac{k_1h}{\xi_1}e_\varphi)^2)+\frac{R_r}{L_r+L_m} \quad (48)$$

$$F_2(e_\omega,\omega_r,\varphi_r)=\frac{J(L_m+L_r)\dot{\omega}_r^*}{2p^2L_m\varphi_r^2}\left(k_\omega e_\omega+k_2\tanh(\frac{k_2h}{\xi_2}e_\omega)-\right.$$
$$\left.\frac{K_f}{J}\omega_r-\dot{\omega}_r^*\right) \quad (49)$$

Finally, the actual control inputs are chosen as follows:

$$v_{sd1}=-\frac{k_{isd1}}{L_{s1}}e_{isd1}-\frac{k_3}{L_{s1}}\tanh(\frac{k_3h}{\xi_3}e_{isd1})+R_{s1}i_{sd1}-\frac{\omega_s}{L_{s1}}i_{sq1}+$$
$$\frac{\tau_r}{2L_{s1}L_m}F_1(e_\varphi)\left(\frac{L_m}{\tau_r}i_{sd}-\frac{1}{\tau_r}\varphi_r\right)+\frac{\tau_r}{2L_{s1}L_m}\ddot{\varphi}_r^*-T_r\varphi_r\omega_s\omega_{gl}-$$
$$\frac{\tau_r}{2L_{s1}L_m}\left[F_1(e_\varphi)-\frac{1}{\tau_r}\right]\dot{\omega}_r^* \quad (50)$$

$$v_{sq1}=-\frac{k_{isq1}}{L_{s1}}e_{isq1}-\frac{k_4}{L_{s1}}\tanh(\frac{k_4h}{\xi_4}e_{isq1})+R_{s1}i_{sq1}+\frac{\omega_s}{L_{s1}}i_{sd1}+$$
$$\frac{J(L_m+L_r)}{2p^2L_{s1}L_m\varphi_r}F_1(e_\omega)\left(\frac{p^2L_m}{J(L_m+L_r)}i_{sq}\varphi_r-\frac{K_f}{J}\omega_r\right)+\omega_s\varphi_r-$$
$$\frac{J(L_m+L_r)}{2p^2L_m\varphi_r}\dot{\omega}_r^*\left(F_1(e_\omega)-\frac{K_f}{J}\right)+\frac{1}{L_{s1}}F_2(e_\omega,\omega,\varphi_r)+$$
$$\frac{(L_m+L_r)K_f^2}{2p^2JL_{s1}L_m\varphi_r}\ddot{\omega}_r^*-\frac{(L_m+L_r)F_1(e_\omega)}{2pL_{s1}L_m\varphi_r}T_L \quad (51)$$

$$v_{sd2}=-\frac{k_{isd2}}{L_{s2}}e_{isd2}-\frac{k_5}{L_{s2}}\tanh(\frac{k_5h}{\xi_5}e_{isd2})+R_{s2}i_{sd2}-$$
$$\frac{\omega_s}{L_{s2}}i_{sq2}-T_r\varphi_r\omega_s\omega_{gl}+\frac{\tau_r}{2L_{s2}L_m}F_1(e_\varphi)\left(\frac{L_m}{\tau_r}i_{sd}-\frac{1}{\tau_r}\varphi_r\right)-$$
$$\frac{\tau_r}{2L_{s2}L_m}\left[F_1(e_\varphi)-\frac{1}{\tau_r}\right]\dot{\omega}_r^*+\frac{\tau_r}{2L_{s2}L_m}\ddot{\varphi}_r^* \quad (52)$$

$$v_{sq2}=-\frac{k_{isq2}}{L_{s2}}e_{isq2}-\frac{k_6}{L_{s2}}\tanh(\frac{k_6h}{\xi_6}e_{isq2})+R_{s2}i_{sq2}+\frac{\omega_s}{L_{s2}}i_{sd2}+$$
$$\frac{J(L_m+L_r)}{2p^2L_{s2}L_m\varphi_r}F_1(e_\omega)\left(\frac{p^2L_m}{J(L_m+L_r)}i_{sq}\varphi_r-\frac{K_f}{J}\omega_r\right)+$$
$$+\frac{(L_m+L_r)K_f^2}{2p^2JL_{s2}L_m\varphi_r}\ddot{\omega}_r^*-\frac{(L_m+L_r)F_1(e_\omega)}{2pL_{s2}L_m\varphi_r}T_L \quad (53)$$

With:

$$\begin{cases}i_{sq}=i_{sq1}+i_{sq2}\\ i_{sd}=i_{sd1}+i_{sd2}\end{cases}$$

The terms $\left\{h_1(x)-\frac{\tau_r}{2L_m}F_1(e_\varphi)h_3(x)\right\}$ and $\left\{h_2(x)-\frac{\tau_r}{2L_m}F_1(e_\varphi)h_3(x)\right\}$ are bounded in the operation domain D defined in [11] since the functions $h_i(x_i):\ i=\overline{1,3}$ are bounded, so we can write:

$$\left|h_1(x)-\frac{\tau_r}{2L_m}F_1(e_\varphi)h_3(x)\right|\le G_1^{\max} \tag{54}$$

$$\left|h_2(x)-\frac{\tau_r}{2L_m}F_1(e_\varphi)h_3(x)\right|\le G_2^{\max} \tag{55}$$

Proposition 1. Let k_{isd1}, k_{isq1}, k_{isd2}, k_{isq2}, k_1, k_2, k_3, k_4, k_5 and k_6 be positive design parameters and let $\xi_1, \xi_2, \xi_3, \xi_4, \xi_5$ and ξ_6 be arbitrary positive small parameters. If $k_1 \ge H_3^{\max}$, $k_2 \ge (p/J)T_L^{\max}$, $k_3 \ge G_1^{\max}$, $k_4>0$, $k_5 \ge G_2^{\max}$ and $k_6>0$, then the dynamical system of tracking errors controlled by (50) – (53) is globally uniformly exponentially practically stable [11].

Proof. The proof consists in showing that the errors variables e_{isd1}, e_{isq1}, e_{isd2}, e_{isq2}, e_φ and e_ω adjusted by the control inputs v_{sd1}, v_{sq1}, v_{sd2} and v_{sq2} presented by (50), (51), (52) and (53), respectively, are globally uniformly exponentially practically stable. Substituting (50) – (53) in (41) – (45), we obtain:

$$\dot{e}_{isd1}=-k_{isd1}e_{isd1}-k_3\tanh\left(\frac{k_3h}{\xi_3}e_{isd1}\right)-\frac{\tau_r}{2L_m}F_1(e_\varphi)h_3(x)+h_1(x) \tag{56}$$

$$\dot{e}_{isq1}=-k_{isq1}e_{isq1}-k_4\tanh\left(\frac{k_4h}{\xi_4}e_{isq1}\right) \tag{57}$$

$$\dot{e}_{isd2}=-k_{isd2}e_{isd2}-k_5\tanh\left(\frac{k_5h}{\xi_5}e_{isd2}\right)-\frac{\tau_r}{2L_m}F_1(e_\varphi)h_3(x)+h_2(x) \tag{58}$$

$$\dot{e}_{isq2}=-k_{isq2}e_{isq2}-k_6\tanh\left(\frac{k_6h}{\xi_6}e_{isq2}\right) \tag{59}$$

$$\dot{e}_\varphi=-k_\varphi e_\varphi+\frac{L_m}{\tau_r}e_d-k_1\tanh\left(\frac{k_1h}{\xi_1}e_\varphi\right)+h_3(x) \tag{60}$$

$$\dot{e}_\omega=\frac{p^2}{J}\frac{L_m}{L_m+L_r}\varphi_r e_{isq}-\frac{p}{J}T_L-k_2\tanh\left(\frac{k_2h}{\xi_2}e_\omega\right)-k_\omega e_\omega \tag{61}$$

Consider the following Lyapunov function:

$$V=\frac{1}{2}(e_{isd1}^2+e_{isq1}^2+e_{isd2}^2+e_{isq2}^2+e_\varphi^2+e_\omega^2)=\frac{1}{2}\|e\|^2 \tag{62}$$

Where $e=\begin{bmatrix}e_{isd1} & e_{isq1} & e_{isd2} & e_{isq2} & e_\varphi & e_\omega\end{bmatrix}^T$.

From step 1 and step 2 we have $k_1 \ge H_3^{\max}$ and $k_2 \ge (p/J)T_L^{\max}$, so for $k_3 \ge G_1^{\max}$, $k_4>0$, $k_5 \ge G_2^{\max}$ and $k_6>0$, we obtain :

$$\dot{V}\le -kV+\xi \tag{63}$$

With

$$\begin{cases}k=2\max\{k_\varphi, k_\omega, k_{isd1}, k_{isq1}, k_{isd2}, k_{isq2}\}\\ \xi=\sum_{i=1}^{6}\xi_i\end{cases}$$

In addition, we have:

$$\left\|\frac{\partial V}{\partial e}\right\|=\|e\|\le\|e\|+b\quad\forall b>0 \tag{64}$$

According to theorem 1 of [11], (63) and (64) imply that the errors variables e_{isd1}, e_{isq1}, e_{isd2}, e_{isq2}, e_φ and e_ω converge to a ball whose radius can be reduced by choosing the setting parameters ξ_i small, with *i={1, 2, 3, 4, 5, 6}*. This means that the error variables are globally uniformly exponentially practically stable. From (20), (33) and (50) – (53), the schematic diagram of the backstepping controller can be represented as in Fig. 3.

5. SIMULATIONS RESULTS

The studied DSIM in this research is powered by two three-phase voltage source inverters (VSIs) using pulse width modulation (PWM) control strategies. The nominal electrical and the mechanical parameters are given in table 1. In steady-state, the machine operates with a fundamental frequency equal to 50 Hz at 100% load. This section shows the performances of the DSIM such as speed, electromagnetic torque, stator current and flux when the machine is operating in a closed loop with a healthy and defective squirrel cage rotor. The startup is done empty under a nominal voltage with a balanced sinusoidal power supply. The reference speed is set at 200 rd/s under a constant load torque of 15 Nm, during the simulation: the value of the reference flux is maintained at 1Wb thanks to a weakening block. The BRB fault is introduced at t = 2 sec. The effectiveness and robustness of the proposed control compared to SMC proposed in [14-15] with different modes of operation, especially in post-fault operation are shown by simulation results using MATLAB/SIMULINK.

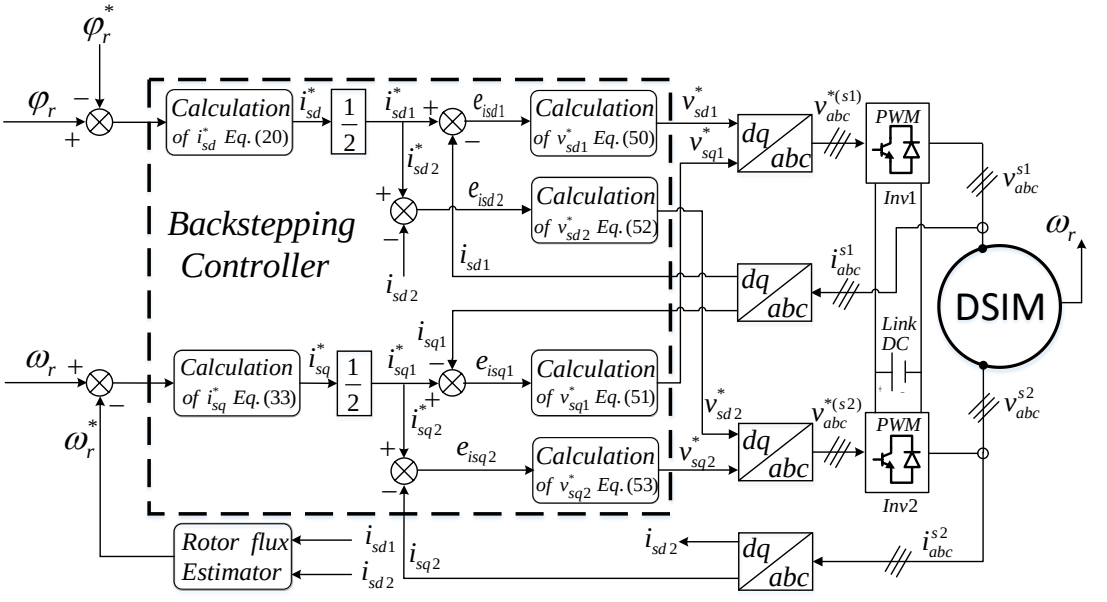

Fig. 3. Backstepping controller design.

Fig.4 below shows the responses of DSIM in healthy and defective operation with SMC proposed in [14-15] and the proposed FTC. The simulation results showed the high performance of the proposed FTC based on the backstepping strategy. The DSIM is starting with a balanced squirrel cage rotor. An external load torque equal to the nominal value is applied at t = 1s.

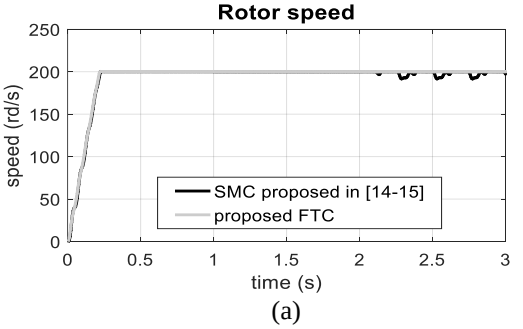

(a)

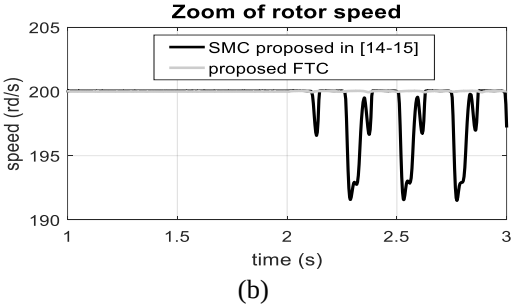

(b)

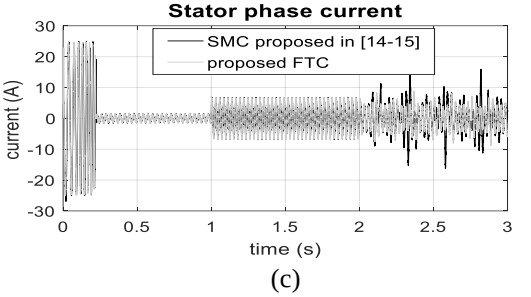

(c)

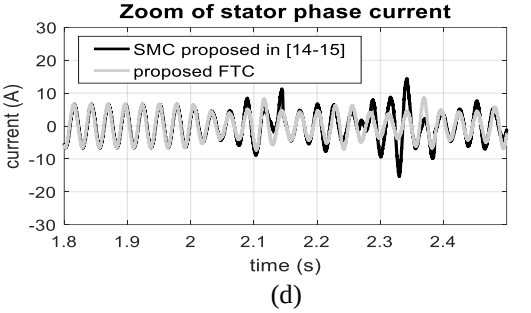

(d)

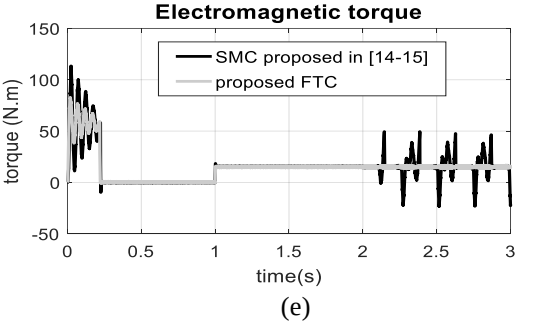

(e)

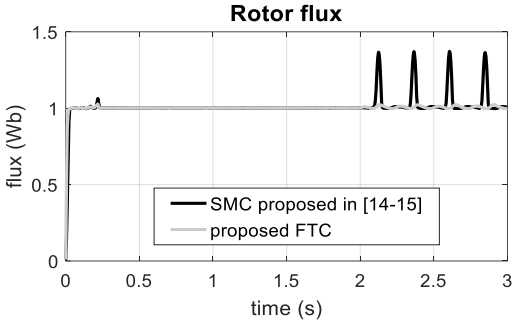

(f)

Fig. 4. Pre-fault (t <2s) and post-fault (t >2s) performance of SMC proposed in [14-15] and proposed FTC for DSIM.

A simulation of the BRB fault is caused at t = 2s. In healthy mode, the speed follows its reference value with neglected overtaking and without oscillations with two control methods, the load torque is very well compensated by the electromagnetic torque (before t = 2s) under rated speed. After the fault occurrence, performance degradation of the DSIM is observed with SMC proposed in [14-15] with closed loop instability; velocity oscillations are visible in Fig. 4.a and Fig. 4.b. The phase current of the stator is not sinusoidal due to the fault effect as shown in Figs. 4.c and Fig. 4.d. High ripples in the electromagnetic torque can be seen in Fig. 5.e, where the maximum positive ripple reaches +49 N.m and the maximum negative ripple reaches -23 N.m. The flux path shown in Fig. 4.f is transformed into oscillations after the appearance of the BRB fault. Regarding the proposed FTC, oscillations of the rotor speed are considerably reduced as indicated in Fig.4.a; the proposed FTC guarantees a better speed response with accurate reference tracking and also provides better stability with the smallest average static error. The tracking performance of the stator current has a small change, according to Fig. 4.c, the current signal is not sinusoidal but it is periodic and symmetrical, moreover, its amplitude does not exceed 10 A, this specific deformation illustrated in Fig. 4.d expresses the compensation of the BRB fault effect by the phases of the stator. Negligible ripples in electromagnetic torque signal are shown in Fig. 4.e. Finally, Fig. 4.f proves that the proposed FTC is capable of correctly driving the flux to its desired reference (1Wb) even in the event of a BRB defect. From these simulation results, we can conclude that the BRB failure does not affect the performance of the proposed FTC, even in the presence of load torque while the SMC proposed in [14-15] is unable to properly handle the machine with an unbalanced squirrel cage rotor.

.

6. CONCLUSION

In this study, a passive fault-tolerant control based on a backstepping strategy for a dual-star induction machine has been developed to ensure robust tracking performance when BRB fault occurs. The effectiveness of the proposed FTC applied on a DSIM with uncertainties is validated using MATLAB / SIMULINK. The results obtained show that the proposed fault-tolerant approach is able to handle post-fault operation and provide a simple configuration but with high performance in terms of speed and torque responses even in case of defective rotor. In addition, the comparative analysis carried out with recent work in the literature, showed the superiority of the proposed FTC that offers better fault tolerance, this PFTC could be a realistic solution and a powerful alternative to existing FTC methods when an efficient fault diagnosis process is difficult to achieve.

Table 1. The machine parameters [2].

Parameter	Definition	Value	Unit
V	Voltage	230-380	V
f	Frequency	50	Hz
$R_{s1} = R_{s2}$	Stator resistance	3.72	Ω
R_r	Rotor resistance	2.12	Ω
$L_{s1}=L_{s2}$	Stator leakage inductance	0.022	H
L_r	Rotor leakage inductance	0.006	H
L_m	Resultant magnetizing	0.3672	H
J	Moment of inertia	0.0662	$kg.m^2$
K_f	Viscous friction coefficient	0.001	$kg.m^2/s$

REFERENCES

[1] Z. Tir, Y. Soufi, M. N. Hashemnia, O. P. Malik, K. Marouani, **"Fuzzy Logic Field Oriented Control of Double Star Induction Motor Drive,"** *Electrical Engineering*, Vol. 99:2, pp. 495-503, 2017.

[2] H. Rahali, S. Zeghlache, L. Benalia, **"Adaptive Field-Oriented Control Using Supervisory Type-2 Fuzzy Control for Dual Star Induction Machine,"** *International Journal of Intelligent Engineering and Systems*, Vol. 10:4, pp. 28-40, 2017.

[3] M. Abd-el-Malek, A. K. Abdelsalam, O. E. Hassan, **"Induction Motor Broken Rotor Bar Fault Location Detection Through Envelope Analysis Of Start-Up Current Using Hilbert Transform,"**, *Mechanical Systems and Signal Processing*, Vol. 93, pp. 332-350, 2017.

[4] R. A. Lizarraga-Morales, C. Rodriguez-Donate, E. Cabal-Yepez, M. Lopez-Ramirez, L. M. Ledesma-Carrillo, E. R. Ferrucho-Alvarez, **"Novel FPGA-based Methodology for Early Broken Rotor Bar Detection and Classification Through Homogeneity Estimation,"** *IEEE Transactions on Instrumentation and Measurement*, Vol. 66:7, pp. 1760-1769, 2017.

[5] E. Elbouchikhi, V. Choqueuse, F. Auger, M. E. H. Benbouzid, **"Motor Current Signal Analysis Based on a Matched Subspace Detector,"** *IEEE Transactions on Instrumentation and Measurement*, Vol. 66:12, pp. 3260-3270, 2017.

[6] Z. Hou, J. Huang, H. Liu, T. Wang, L. Zhao, **"Quantitative Broken Rotor Bar Fault Detection for Closed-Loop Controlled Induction Motors,"** *IET Electric Power Applications*, Vol. 10:5, pp. 403-410. 2016.

[7] K. M. Sousa, I. B. V. da Costa, E. S. Maciel, J. E. Rocha, C. Martelli, J. C. C. da Silva, **"Broken Bar Fault Detection in Induction Motor by Using Optical Fiber Strain Sensors,"** *IEEE Sensors Journal*, Vol. 17:12, pp. 3669-3676, 2017.

[8] C. Lebreton, C. Damour, M. Benne, B. Grondin-Perez, J. P. Chabriat, **"Passive Fault Tolerant Control of PEMFC Air Feeding System,"** *International Journal of Hydrogen Energy*, Vol. 41:34, pp. 15615-15621, 2016.

[9] C. H. Xie, G. H. Yang, **"Data-based Fault-Tolerant Control for Affine Nonlinear Systems With Actuator Faults, "** *ISA transactions*, Vol. 64, pp. 285-292, 2016.

[10] Y. Zhang, S. Tang, J. Guo, **"Adaptive-gain Fast Super-Twisting Sliding Mode Fault Tolerant Control for A Reusable Launch Vehicle In Reentry Phase,"** *ISA transactions*, Vol. 71: (Pt 2), pp. 380-390, 2017.

[11] N. Djeghali, M. Ghanes, S. Djennoune, J. P. Barbot, **"Sensorless fault Tolerant Control for Induction Motors, "** *International Journal of Control, Automation and Systems*, Vol. 11:3, pp. 563-576, 2013.

[12] H. Echeikh, R. Trabelsi, A. Iqbal, N. Bianchi, M. F. Mimouni, **"Comparative Study Between The Rotor Flux Oriented Control And Non-Linear Backstepping Control of A Five-Phase Induction Motor Drive–An Experimental Validation, "** *IET Power Electronics*, Vol. 9:13, pp. 2510-2521, 2016.

[13] H. Echeikh, R. Trabelsi, A. Iqbal, N. Bianchi and M. F. Mimouni, **"Non-linear Backstepping Control of Five-Phase IM Drive at Low Speed Conditions–Experimental Implementation,"** *ISA transactions*, Vol. 65, pp. 244-253, 2016.

[14] J. Listwan, K. Pieńkowski, **"Sliding-mode Direct Field-Oriented Control of Six-Phase Induction Motor,"** *Technical Transactions*, Vol. (2-M), pp. 95-108, 2016.

[15] M. A. Fnaiech, F. Betin, G. A. Capolino, F. Fnaiech, **"Fuzzy Logic And Sliding-Mode Controls Applied to Six-Phase Induction Machine with Open Phases,"** *IEEE Transactions on Industrial Electronics*, Vol. 57:1, pp. 354-364, 2010.

[16] S. Cho, Z. Gao, T. Moan, **"Model-based Fault Detection, Fault Isolation and Fault-Tolerant Control of A Blade Pitch System In Floating Wind Turbines,"** *Renewable Energy*, Vol. 120, pp. 306-321, 2018.

[17] H. Mekki, O. Benzineb, D. Boukhetala, M. Tadjine, M. Benbouzid, **"Sliding Mode Based Fault Detection, Reconstruction and Fault Tolerant Control Scheme for Motor Systems,"** *ISA transactions*, Vol. 57, pp. 340-351, 2015.

[18] K. Xiahou, M. S. Li, Y. Liu, Q. H. Wu, **"Sensor Fault Tolerance Enhancement of DFIG-WTs via Perturbation Observer-based DPC and Two-Stage Kalman Filters, "** *IEEE Transactions on Energy Conversion*, Vol. 33:2, pp. 483-495, 2017.

[19] I. González-Prieto, M. J. Duran, F. J. Barrero, **"Fault-Tolerant Control Of Six-Phase Induction Motor Drives with Variable Current Injection, "** *IEEE Transactions on Power Electronics*, Vol. 32:10, pp. 7894-7903, 2017.

[20] E. A. Mahmoud, A. S. Abdel-Khalik, H. F. Soliman, **"An Improved Fault Tolerant for A Five-Phase Induction Machine under Open Gate Transistor Faults, "** *Alexandria Engineering Journal*, Vol. 55:3, pp. 2609-2620, 2016.

[21] S. Bednarz, **"Rotor Fault Compensation and Detection in a Sensorless Induction Motor Drive,"** *Power Electronics and Drives*, Vol. 2:1, pp. 71-80, 2017.